

PairingNet: A Learning-based Pair-searching and -matching Network for Image Fragments

Rixin Zhou¹ Ding Xia² Yi Zhang³ Honglin Pang¹ Xi Yang^{1,4,5,*} Chuntao Li^{5,6,*}
¹School of Artificial Intelligence, Jilin University ²The University of Tokyo
³National University of Defense Technology, College of Electronic Engineering
⁴Engineering Research Center of Knowledge-Driven Human-Machine Intelligence, MoE, China
⁵Key Laboratory of Ancient Chinese Script, Culture Relics and Artificial Intelligence, Jilin Province
⁶School of Archaeology, Jilin University

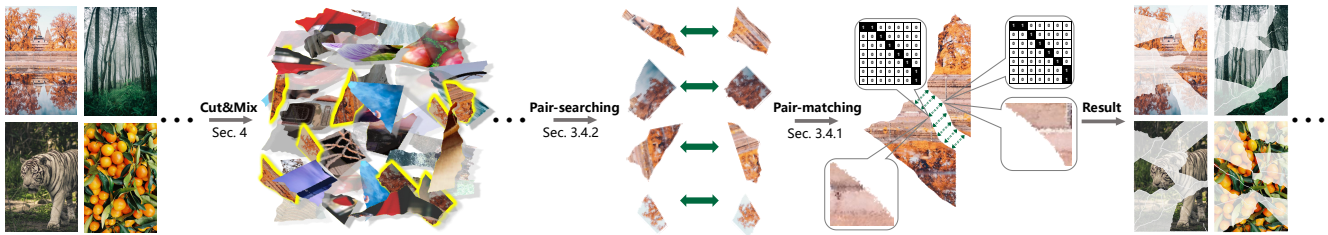


Figure 1. Our pair-searching and -matching task. Given a large number of mixed image fragments, our proposed network can search and match pairs of fragments, which is important for restoration problems. We also designed an algorithm to generate a dataset of image fragments by tearing a set of complete images.

Abstract

In this paper, we propose a learning-based image fragment pair-searching and -matching approach to solve the challenging restoration problem. Existing works use rule-based methods to match similar contour shapes or textures, which are always difficult to tune hyperparameters for extensive data and computationally time-consuming. Therefore, we propose a neural network that can effectively utilize neighbor textures with contour shape information to fundamentally improve performance. First, we employ a graph-based network to extract the local contour and texture features of fragments. Then, for the pair-searching task, we adopt a linear transformer-based module to integrate these local features and use contrastive loss to encode the global features of each fragment. For the pair-matching task, we design a weighted fusion module to dynamically fuse extracted local contour and texture features, and formulate a similarity matrix for each pair of fragments to calculate the matching score and infer the adjacent segment of contours. To faithfully evaluate our proposed network, we created a new image fragment dataset through an algorithm we designed that tears complete images into irregular fragments. The experimental results show that our proposed network achieves excellent pair-searching accuracy, reduces matching errors, and significantly reduces computational time. Details, sourcecode, and data are available in our supplementary material.

1. Introduction

Pair-searching and -matching of massive unorganized fragments is a critical problem in the research fields of computer vision and computer graphics, especially in the field of cultural relic restoration [1, 11, 15, 22]. Traditional methods achieve geometry transformation between fragments by calculating the similarity of contour segments based on geometric invariants such as curvature and manually designed descriptors [18, 30]. It has a common core with the registration problem [3], which is to establish the correspondences of local features between related image pairs of the same scene. However, fragment assembly is more challenging because they do have overlapping regions. Thus, existing rule-based methods are difficult to generalize to various complex situations. Furthermore, they are time-consuming since the computational complexity of finding matching pairs from a set of fragments is typically $O(N^2)$ in global search, and in practice, only a few pairs are hidden in a large number of mixed fragments.

Solving jigsaw puzzles [14, 34, 39] is also a similar task and learning-based approaches have been applied [2, 33]. However, there are two differences that make these algorithms not generalizable. First, puzzle pieces usually have regular shapes, so they are best matched based on content information rather than contour features. Second, this problem usually studies matching all fragments into a complete block. Their input fragments do not come from mixed

*Corresponding authors

groups, and the matching results are dense and not lost. Therefore, they often use neighbor relationships to build graphs to constrain the search for the correct alignment of fragments. Once a fragment is lost, their closed-loop strategy fails.

In this paper, we propose PairingNet, an end-to-end deep learning network, for searching and matching pairs from a large number of image fragments. To address this problem, we first explore the use of Graph Convolutional Networks (GCNs) to extract more robust contour and texture features for our tasks. Second, we design a feature fusion way to learn local matching features by calculating the similarity matrix of each fragment pair. Third, we build a module based on the linear transformer to learn the global searching features for fragments using contrastive learning. Finally, we generate a large-scale image fragment dataset to provide data-driven and validate the effectiveness of our proposed network. The main contributions of our work are as follows:

- We propose a novel network to leverage the local contour and texture features for solving the pair-searching and -matching of image fragments. It provides an attempt to use advanced deep-learning techniques to solve this long-standing problem.
- We provide a new dataset with a carefully designed algorithm to simulate real-world fragments. The algorithm generates various types of image fragments to facilitate the application of subsequent learning-based methods.
- We conduct extensive experiments, ablation studies, and visual analysis to demonstrate the effectiveness of our proposed network.

2. Related Work

2.1. Fragments Assembly (Irregular Shape)

Here we focus on the pairwise matching algorithms of related representative works, although few of them also consider fragment relationships. Methods based on deep neural networks have been studied for object fragments; however, we could not find representative works for image fragments or even suitable datasets.

Image fragments. Kong and Kimia [24] solved fragment matching using geometric features (partial curve matching). Leitao and Stolfi [11] described a specific multiscale matching method for the reassembly of 2D fragmented objects. Tsamoura and Pitas [40] presented a color-based method to automatically reassemble image fragments. Huang et al. [21] relied on salient curves detected inside the different image pieces to align gapped fragments. Subsequently, both shape and appearance information along the boundaries were utilized and extracted for each piece for matching [29, 47]. Furthermore, Derech et al. [12] proposed to

extrapolate each fragment to address fragment abrasion. For learning-based methods, traditional machine learning (SVM/Random Forest) was used as a classifier to process extracted local features [1, 35]. Then Le and Li [26] built a deep convolutional neural network to detect the compatibility of pairwise stitching.

Object fragments. Huang et al. [22] analyzed the geometry of the fracture surfaces by computing multi-scale surface characteristics. Yang et al. [44] matched stone tools based on contour points and their mean normals. Funkhouser et al. [15] learned a decision tree classifier to filter the candidates. Hong et al. [20] solved the problem of indistinguishable false matches by employing beam search to explore multiple registration possibilities. Ye et al. [45] presented an immersive system that can handle complex and ambiguous fragment shapes interactively with experts. In recent years, deep learning networks have been rapidly applied in 3D assembly. Huang et al. [46] proposed an assembly-oriented dynamic graph learning framework to estimate the pose of 3D parts. Chen et al. [8] proposed Neural Shape Mating (NSM) to tackle pairwise 3D geometric shape mating. Wu et al. [43] leveraged SE(3) equivariance for such shape pose disentanglement.

Datasets. Existing image assembly works typically collect data in two ways: manual digitalization by photographing or scanning broken fragments, or using simple algorithms to tear complete images [6, 32, 35]. The lack of a large-scale dataset prevents the emergence of deep learning networks for this task. However, multiple datasets have been introduced in 3D assembly problems [23, 25, 37].

2.2. Jigsaw Puzzles (Regular Shape)

Solving jigsaw puzzles was first proposed in [14], and then regular pieces became a key research object in computer vision. Many existing methods [10, 16, 19, 34, 38, 39] focused on building relationships of pieces based on content information rather than contour-based pair-searching/-matching. And deep learning techniques [2, 33] was also used to solve this problem.

3. Method

3.1. Problem Statement

Let us consider a fragment dataset $\mathbf{F} = \{f^{(i)}\}_{i=1}^N$, which consists of fragments f torn from a certain image dataset. We define the contour points $c_j^{(i)} \in \mathbf{C}^{(i)}$ for each $f^{(i)}$, where $j = 1, 2, \dots, M^{(i)}$, $M^{(i)}$ is the contour length and $\mathbf{C}^{(i)}$ is an ordered set that contains all contour points of $f^{(i)}$.

Regarding any two neighbor fragments sampled from a pairset \mathbf{P} , we denote the pair as $f^{(m)}$ and $f^{(n)}$. The *pair-searching task* aims to retrieve the pairset \mathbf{P} from a given

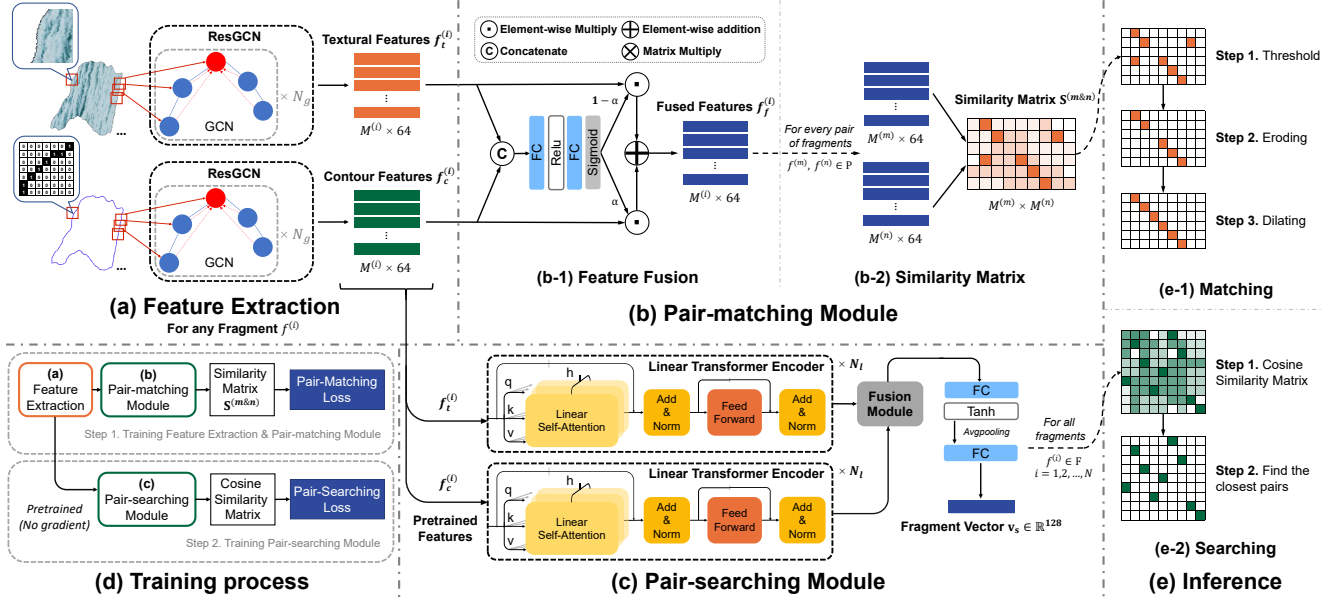


Figure 2. Pipeline of our proposed PairingNet. (a) Based on patches, we first employ a binary encoding to describe contours and use ResGCN as the backbone to extract the local contour and texture features of image fragments. (b) We design self-gated fusion to fuse the extracted features in a weighted manner to calculate the similarity matrix for each pair of fragments, and (c) a linear transformer-based encoder for learning the global features of each fragment. (d) We use a two-step strategy to train our proposed network. (e) During inference, we calculate Cosine similarity to find the adjacent fragment pairs and further process the matching similarity matrix to establish better correspondences between a fragment pair.

fragment dataset \mathcal{F} . Meanwhile, for the contours of the paired fragments, $\mathcal{C}^{(m)}$ and $\mathcal{C}^{(n)}$, we can always find the overlapped part $\mathcal{C}^{(m&n)}$. The *pair-matching* task is designed to find the adjacent part from any given fragment pair.

3.2. Network Architecture

In the *pair-matching* task, a model has the capability to discern differences between two fragments, regardless of whether these discrepancies are on a large or minimal scale. Simultaneously, the features extracted by the model can be used to quantify the likelihood of adjacency between any given two fragments, assisting in the identification of matched pairs. However, the process of comparing every two fragments is not only laborious, but also inefficient. Therefore, utilizing the rich features the *matching model* extracts, we conceived a *pair-searching* module. This innovative module can adeptly convert any fragment into a unique feature vector, thereby significantly accelerating the pair-searching process.

3.2.1 Feature Extraction

Contour encoding. In this module, we aim to direct the model’s attention to the unique features of contours. We design distinct contour encodings that also may be applied

in other sketch-based fields. We tested various patch sizes and all these distinct encodings, finalizing a binary encoding and a patch size of 7×7 for our network. Subsequently, these contour patches are processed through a convolutional layer, followed by an average pooling layer and a fully connected network. We then adopt ResGCN [27] to amalgamate adjacent features, further extracting comprehensive global features. As such, for any provided fragment input denoted as $f^{(i)}$ with its corresponding contour $\mathcal{C}^{(i)}$, this module yields a return of $f_c^{(i)} \in \mathbb{R}^{M^{(i)} \times 64}$.

Textural encoding. Our objective is to accentuate the distinguishing characteristics of textures in this module. We begin by cropping the image using a patch centered on each contour point. This is followed by filtering these patches through two consecutive convolutional layers, coupled with a single average pooling operation. Then, a ResGCN [27] is integrated to compile adjacent features, thereby enhancing the receptive domain of local textural characteristics. For any given fragment input represented as $f^{(i)}$ along with its associated contour $\mathcal{C}^{(i)}$, this module produces an output of $f_t^{(i)} \in \mathbb{R}^{M^{(i)} \times 64}$.

3.2.2 Pair-matching Module

Feature Fusion. Regarding the decision-making process for pair-matching and -searching tasks, the dependence on

contour and textural features varies. For instance, in scenarios where both fragments are solid colors, texture serves as the primary identifying factor suggesting adjacency. However, texture alone cannot identify the matched contours. In contrast, simple contours, like straight lines, require texture features for accurate matching position determination, as contour information alone falls short.

Given this, we propose the incorporation of a *Feature Fusion* module which would be capable of adaptively fine-tuning the weights assigned to these two features. The specific structure of this integral component is depicted in Figure 2 (b). First, we concatenate $f_t^{(i)}$ and $f_c^{(i)}$, then the weight $\mathbf{w}^{(i)}$ for each contour point $c_j^{(i)} \in \mathbf{C}^{(i)}$ is computed by:

$$\mathbf{w}^{(i)} = \sigma(\mathbf{W}_g(f_t^{(i)} \odot f_c^{(i)}) + \mathbf{b}_g)^{(i)} \quad (1)$$

where σ is *sigmoid* the activation function, \odot means channel-wise concatenation, and $\mathbf{w} \in \mathbb{R}^{M^{(i)} \times 64}$. Second, we fuse features of two modalities:

$$\mathbf{F}_f^{(i)} = \mathbf{w}^{(i)} \odot \mathbf{F}_t^{(i)} + (1 - \mathbf{w}^{(i)}) \odot \mathbf{F}_c^{(i)} \quad (2)$$

where $\mathbf{F}_f^{(i)} \in \mathbb{R}^{M^{(i)} \times 64}$, and \odot is element-wise multiplication. With this module, we let the model adaptively decide the weights between textual and contour features, which is proven effective in later experiments.

Similarity Matrix. For every pair of fragments $f^{(m)}$ and $f^{(n)}$ from the pairset \mathbf{P} with contour points $\mathbf{C}^{(m)}$ and $\mathbf{C}^{(n)}$, we are able to formulate the similarity matrix $\mathbf{S}^{(m\&n)} \in \mathbb{R}^{M^{(m)} \times M^{(n)}}$ [9, 36].

We first calculate the similarity matrix $\hat{\mathbf{S}}^{(m\&n)}$ by simple matrix multiplication:

$$\hat{\mathbf{S}}^{(m\&n)} = \frac{1}{\sqrt{D}} \mathbf{F}_f^{(m)} (\mathbf{F}_f^{(n)})^T \quad (3)$$

where D is the dimension of the feature, in our model, D is 64. Then, each entry in the matrix $\mathbf{S}^{(m\&n)}$ is normalized:

$$\mathbf{S}^{(m\&n)}(i, j) = \frac{\exp(\hat{\mathbf{S}}_{i,j}^{(m\&n)})}{\sum_i \exp(\hat{\mathbf{S}}_{i,j}^{(m\&n)})} \frac{\exp(\hat{\mathbf{S}}_{i,j}^{(m\&n)})}{\sum_j \exp(\hat{\mathbf{S}}_{i,j}^{(m\&n)})} \quad (4)$$

3.2.3 Pair-searching Module

We introduce a modified feature fusion module to process features extracted by the backbone network and encode any fragment $f^{(i)}$ into a feature vector $v_s^{(i)} \in \mathbb{R}^{128}$. It is based on the discovery that using fused features in the pair-matching task will lower the performance.

To be specific, every feature branch utilizes a Linear Transformer Encoder [41] to enhance the encoding of both contour and textural features. Subsequent to the modified fusion module, we add a fully-connected layer to encode the fused feature regarding per contour point. Then an average pooling layer is applied to map the feature matrix to

a singular vector. Finally, another fully-connected layer is used to encode the feature.

For every pair of fragment $f^{(i)}$ and $f^{(j)}$ from the fragment set \mathbf{F} , this module allows them to be encoded as $v_s^{(i)}$ and $v_s^{(j)}$. By calculating their inner product, we can efficiently quantify and contrast their similarity, thereby expeditiously identifying neighbor pairs.

3.3. Loss Function

3.3.1 Pair-matching Loss

Given the extreme imbalance in the ratio of positive to negative samples in the pair-matching task, we adopt the concept of focal loss [28] to concentrate on learning challenging correspondences.

For any paired fragments $f^{(m)}$ and $f^{(n)}$, entries in the ground truth similarity matrix $\mathbf{S}_{gt}^{(m\&n)}$ are 1 for matched contour points and 0 for unmatched ones. We calculate the matching loss $\mathcal{L}_{match}^{(m\&n)}$ as follows:

$$\begin{aligned} \mathcal{L}_{match}^{(m\&n)} = & \text{SUM}(\beta_1(1 - \mathbf{S}^{(m\&n)})^\gamma \log \mathbf{S}^{(m\&n)} \mathbf{S}_{gt}^{(m\&n)}) \\ & + \beta_2(\mathbf{S}^{(m\&n)})^\gamma \log(1 - \mathbf{S}^{(m\&n)})(1 - \mathbf{S}_{gt}^{(m\&n)}) \end{aligned} \quad (5)$$

where β_1 and β_2 are the balancing weights and $\beta_1 + \beta_2 = 1$, γ is the decay factor, SUM is a function that adds all the entries in the input matrix, and all operations except SUM are element-wise. By calculating and adding the pair-matching loss for all paired fragments $f^{(m)}$, $f^{(n)}$ from the pairset \mathbf{P} , we get \mathcal{L}_{match} .

3.3.2 Pair-searching Loss

In the pair-searching task, we employ InfoNCE loss [31] as the contrastive loss function \mathcal{L}_{search} . Contrary to the scenario of self-supervised learning [7], where data samples and noise samples are used to construct positive sample pairs, we utilize paired samples for constructing positive sample pairs, and unpaired samples for constructing negative sample pairs.

3.4. Inference

3.4.1 Pair-matching

In this section, we target to retrieve matched contour from the similarity matrix $\mathbf{S}^{(m\&n)}$.

We first apply a threshold $\epsilon = 0.006$ to filter out noisy entries. Entries with value lower than the threshold is set to 0. Because contour pointset $\mathbf{C}^{(m)}$ and $\mathbf{C}^{(n)}$ are ordered sets, for any ground truth similarity matrix $\mathbf{S}_{gt}^{(m\&n)}$, if the start for contour points is the left-top corner, we can observe that the part with a value of 1 in the matrix must be arranged in the direction from upper left to lower right and connected into a line segment. Therefore, this inspires us to enhance

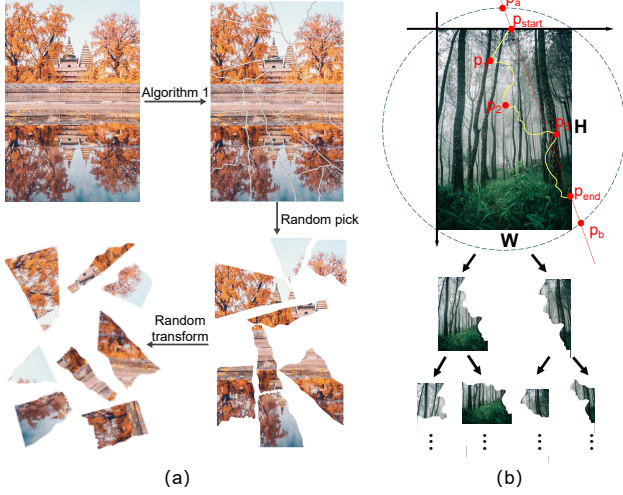


Figure 3. Dataset creation. (a) The process of generating our dataset. (b) Illustration of Algorithm 1 for tearing a complete image.

the filtered similarity matrix. We design an eroding kernel \mathbf{K}_e to filter out not dominant segments, which is adopted once. Then a dilating kernel \mathbf{K}_d is applied once to connect close but split segments. The definitions of two kernels are as follows:

$$\mathbf{K}_e = \begin{bmatrix} 0 & 0 & 1 \\ 0 & 0 & 0 \\ 1 & 0 & 0 \end{bmatrix}, \quad \mathbf{K}_d = \begin{bmatrix} 0 & 0 & 1 \\ 0 & 1 & 0 \\ 1 & 0 & 0 \end{bmatrix}. \quad (6)$$

Finally, we use RANSAC [13] to estimate the correspondences of two fragments and obtain the transformation matrix.

3.4.2 Pair-searching

For N fragments $f^{(i)} \in \mathbf{F}, i = 1, 2, \dots, N$, using the searching module, we can get a feature matrix $\mathbf{V}_s \in \mathbb{R}^{N \times 128}$. Subsequently, we compute the cosine similarity between all global features to form the cosine similarity matrix. This allows us to obtain the similarity score for any pair of fragments.

4. Dataset

We design Algorithm 1 to tear a series of complete images and create a new image fragment dataset with data close to the real world. The process is also shown in Figure 3. To control the shape and area of the fragments, we first find the circumscribed circle of a fragment and take two points at an appropriate distance on the circle to determine the starting and ending points of the segmentation. Then, to simulate a more realistic fragment contour, we randomly divide the cutting line into several segments, each segment

Algorithm 1 Generate fragments of an image

Input: List of fragments $L_{frag} = \{\}$, a complete image I ;
 Max iterations $t_{max} = 40$, min arc length ratio $\tau = 0.9$, max number of cutting points $N_{max} = 3$, min distance from cutting point to edge of fragment $D_{min} = 100$, the number of Fourier orthogonal basis $n = 20$, scaling ratios $s_1 = 0.25, s_2 = 0.0067, s_3 = 1.5, s_4 = 0.3$, probability of curve type $\rho = 0.5$, mini fragment size $h_{min} = 150, w_{min} = 150$.

Output: Collection of fragments L_{frag}

```

1: put  $I$  in  $L_{frag}$ 
2: while  $t < t_{max}$  do
3:    $f \leftarrow$  randomly_pick( $L_{frag}$ ),  $R \leftarrow$  bounding_rectangle( $f$ )
4:    $W, H \leftarrow$  width_and_height( $R$ ),  $C \leftarrow$  circumscribed_circle( $R$ )
5:    $l_{dia} \leftarrow$  diameter( $C$ )
6:
7:   // generate the cutting points
8:   repeat
9:      $p_a, p_b \leftarrow$  randomly_pick( $C$ )
10:     $l_{arc} \leftarrow$  smaller_arc_length( $p_a, p_b$ )
11:    until  $l_{arc} > \tau \cdot l_{per}$ 
12:     $p_{start}, p_{end} \leftarrow$  intersection( $f, p_a, p_b$ )
13:     $m \leftarrow$  randomly_pick $\{0, \dots, N_{max}\}$ 
14:    repeat
15:       $[p_1, \dots, p_m] \leftarrow$  random_select_inside_points( $f, m$ )
16:       $d \leftarrow$  min_distance_to_edge( $f, p_1, \dots, p_m$ )
17:    until  $d > D_{min}$ 
18:    put  $p_{start}, p_{end}$  in  $[p_1, \dots, p_m]$ 
19:
20:   // generate the cutting segments
21:   for each  $p_i \in [p_{start}, p_1, \dots, p_m, p_{end}]$  do
22:     irregular line  $l_{irr} = \{\}$ , phase  $\phi \sim \mathcal{U}(-\pi, \pi)$ ,
23:     amplitude  $A \sim \mathcal{N}(s_1 H, s_2 H)$ , period  $T \sim \mathcal{N}(s_3 W, s_4 W)$ 
24:     for each  $x$ -coordinate between  $(p_i, p_{i+1})$  do
25:        $y \leftarrow \sum_{i=0}^n \frac{A}{1+i} \sin(\frac{2\pi i}{T} x + \phi) + \frac{H}{2}$ 
26:       put  $\{x, y\}$  in  $l_{irr}$ 
27:     end for
28:      $l_{str} \leftarrow$  straight_line( $p_i, p_{i+1}$ )
29:      $l_{cut} \leftarrow$  select_and_connect( $l_{irr}, l_{str}, \rho, l_{cut}$ )
30:   end for
31:    $f_1, f_2 \leftarrow$  cut_fragment( $f, l_{cut}$ )
32:   if size( $f_1$ )  $> h_{min}, w_{min}$  and size( $f_2$ )  $> h_{min}, w_{min}$  then
33:     put  $f_1, f_2$  in  $L_{frag}$ 
34:   end if
35: end while

```

Table 1. Dataset division. We divide the entire test set into three difficulty levels according to the contour overlapping proportion of fragment pairs.

	Total	Train	Validation	Test			
				Full	High	Medium	Low
Fragments	8196	4098	819	3279	1071	1671	1090
Pairs	14951	3654	137	2370	663	1103	604

randomly choosing a straight line or an irregular curve. The irregular curve is synthesized by a series of Fourier orthogonal bases to make the shape of the fragments more abundant and closer to the edge of a real torn paper. We set a minimum threshold for the fragments, and the fragment is re-segmented if a very small fragment appears.

To create our dataset, we collect 390 images of ten themes from Pexels [4] and empirically set the generation

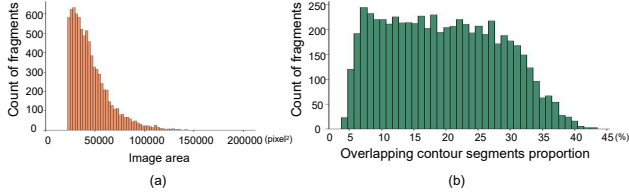


Figure 4. Dataset statistics. (a) Image area distribution of the generated fragments. (b) Proportional distribution of overlapping contour segments.

parameters shown in Algorithm 1 to obtain fragments. We calculate the distributions of our generated data, as shown in Figure 4. The distribution of fragment areas exhibits a long-tail pattern, which is consistent with the distribution of fragment areas observed when tearing large amounts of paper in real-life scenarios. The contour overlapping proportion of fragment pairs is closer to a uniform distribution over most ranges, indicating that our algorithm generates various types of fragment pairs. Then, we divide the dataset into training set, validation set, and test set in 5:1:4. We further divide the full test set into three difficulty levels based on the overlapping proportion of contour segments between fragment pairs. Low difficulty means that the pair of fragments has larger overlapping contour segments, and vice versa. The details are shown in Table 1.

5. Experiments

5.1. Comparison Methods

Finding comparison methods is not easy. Because rule-based methods have been around for quite some time, lack source code, and tend to exhibit lower performance compared to advanced deep learning methods. However, most existing deep learning methods require extensive modifications if applied to our task. Therefore, we employ Jigsawnet [26] (without loop consistency) and a rule-based method [47] (Step 1) as our comparison methods.

5.2. Implementation Details

Our PairingNet was implemented by PyTorch, and conducted on a server with 4 RTX A40 GPUs and Intel® Xeon® Gold 5220 CPUs (72 cores). We used the Adam optimizer with an initial learning rate of 0.001, which was adjusted using a cosine annealing strategy. For training pair-matching module, the batch size was set to 20, and for the pair-searching module, the batch size was set to 175.

For comparison methods, we used the official source-code (implemented by TensorFlow) of Jigsawnet and conducted experiments on a server with 4 Quadro RTX 6000 GPUs and Intel® Xeon® Gold 5220 CPUs (144 cores). We reproduced the rule-based method by Python and conducted experiments on a node of a Supercomputing platform with

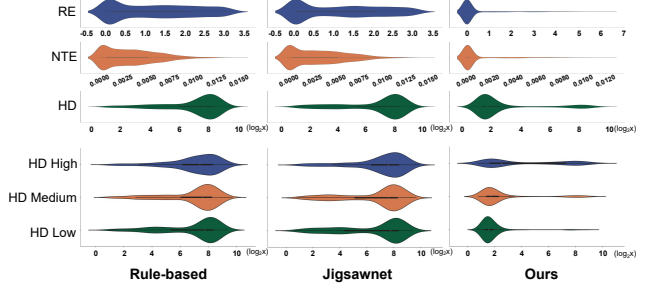


Figure 5. Violin plots of the matching results of our method and the comparison method: (a) RE, NTE, and HD on the test set. (b) HD on the test sets of different difficulties.

Intel® Xeon® Gold 6258R CPUs (128 cores).

For evaluation metrics, we employ Recall@k and NDCG@k [5] for the pair-searching task, and Registration recall (RR), Hausdorff distance (HD), Radians Error (RE) and Normalized Translation Error (NTE) for the pair-matching task. Here, we normalize Translation Error (TE) by the sum of the areas of fragment pairs to obtain the NTE, considering the large difference in area between fragments.

5.3. Results

Performance. As shown in Table 2, our network outperforms the comparison methods on both the full test set and on every set of difficulty levels. Jigsawnet shows a certain superiority in pair-searching on the high-difficulty set, probably because it treats the problem as a simple binary classification task; however, their pair-matching results are very unsatisfactory. It should be noted that we did not evaluate Recall@1 and NDCG@1 here due to the many-to-many pairings in our dataset, making it unreasonable to search only for the fragment with the highest similarity of searching. We can also observe that the performance of our proposed network shows reasonable variation with the difficulty of the data. This shows that our proposed network learns useful information and has more potential in complex situations. However, Jigsawnet and the rule-based method show relatively identical performance on test sets of different difficulty levels. Furthermore, we also plot the distributions of HD, RE, and NTE for each method for a more intuitive comparison, as shown in Figure 5.

Inference time. We test the inference time of different methods on the pair-searching task on our generated test set. As shown in Figure 6, our network is significantly faster than the comparative methods. Our network retrieves all fragment pairs in 73 seconds, while the rule-based method takes 223 hours, and Jigsawnet takes 10 hours. For ease of presentation, we have plotted the logarithm of the inference time for the pair-searching task.

Table 2. Comparison Results of various metrics. The best results in our full dataset are highlighted in bold font, and the best results for each difficulty are marked in different colors.

Method	Difficulty	Recall@5	Recall@10	Recall@20	NDCG@5	NDCG@10	NDCG@20	RR ↑	HD ↓	RE ↓	NTE ↓
Rule-based	High	0.261	0.354	0.443	0.185	0.218	0.241	0.107	212.003	1.289	37.100×10^{-4}
	Medium	0.329	0.427	0.529	0.242	0.275	0.302	0.153	205.463	1.249	33.742×10^{-4}
	Low	0.358	0.464	0.555	0.261	0.296	0.32	0.188	210.274	1.231	32.692×10^{-4}
	All	0.317	0.416	0.511	0.248	0.284	0.311	0.149	208.519	1.256	34.414×10^{-4}
Jigsawnet	High	0.305	0.394	0.478	0.231	0.261	0.284	0.117	226.026	1.306	37.011×10^{-4}
	Medium	0.383	0.478	0.565	0.309	0.34	0.364	0.213	206.040	1.155	31.467×10^{-4}
	Low	0.459	0.548	0.631	0.368	0.397	0.419	0.241	202.942	1.186	30.500×10^{-4}
	All	0.38	0.472	0.557	0.326	0.359	0.383	0.194	210.842	1.205	32.772×10^{-4}
Ours	High	0.276	0.413	0.535	0.189	0.234	0.268	0.606	92.229	0.807	18.335×10^{-4}
	Medium	0.501	0.619	0.732	0.382	0.423	0.454	0.879	35.617	0.236	5.685×10^{-4}
	Low	0.717	0.805	0.879	0.581	0.61	0.629	0.961	12.336	0.09	1.936×10^{-4}
	All	0.493	0.608	0.714	0.417	0.458	0.487	0.835	43.116	0.352	7.735×10^{-4}

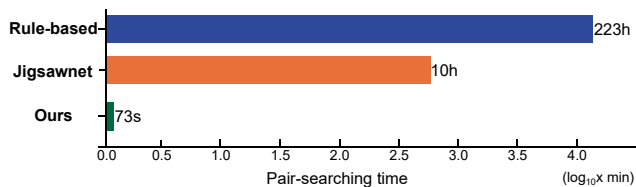


Figure 6. Total inference time for different methods on the pair-searching task. This comparison is numerically unfair because the experiments were performed on different devices; however, it is useful in practice.

Visualization. We show the top five search results of different methods for the examples of fragment pairs in Figure 7. Given a source fragment, our model can accurately identify the corresponding target fragment (marked with a green box). Furthermore, in situations where a source fragment can be paired with multiple target fragments, our method identifies all matching fragments within the top five search results. We also show examples of matching results for three difficulty levels in Figure 8. Our method produces matching results that are consistent with the Ground Truth (GT), while the comparison methods yield numerous incorrect results.

We also visualize the normalized self-gated weights to analyze their changes under different situations. As shown in Figure 9 (a), we map the normalized weights to the edges of the fragments to show the influence of the texture/contour features. We classify the local parts of fragments into four types based on the information contained in texture and contour: those with rich texture and contour information (first quadrant), those with rich texture information (second quadrant), those with little texture and contour information (third quadrant), and those with rich contour information but with little texture information (fourth quadrant). The red color indicates that the weights of the texture features are relatively large, while the green indicates that the contour feature weights are relatively large. The results show that our proposed network learned varying weights of the

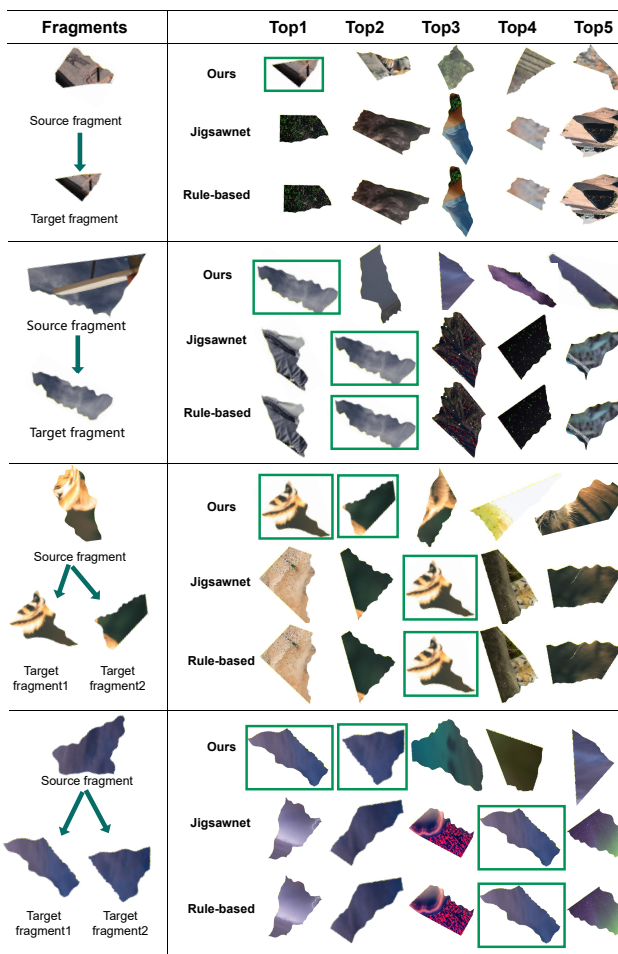


Figure 7. Examples of pair-searching results. Our network is able to accurately identify the corresponding target fragment (highlighted with a green box).

features for fragments with different characteristics.

5.4. Ablation Study

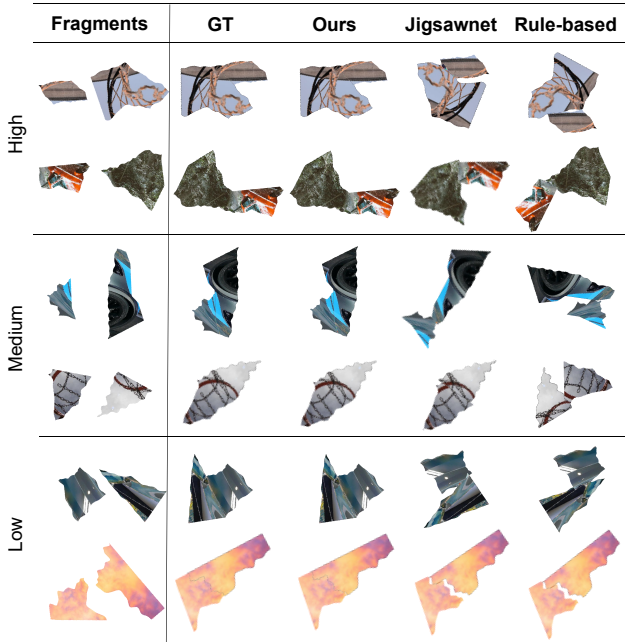


Figure 8. Examples of pair-matching results for three difficulty levels. Our proposed network achieves satisfactory matching results. However, for low-difficulty cases, Jigsawnet and the Rule-based method find approximate matching positions, while the matchings are not accurate enough. For medium- and high-difficulty cases, both comparison methods are difficult to obtain correct matching results.

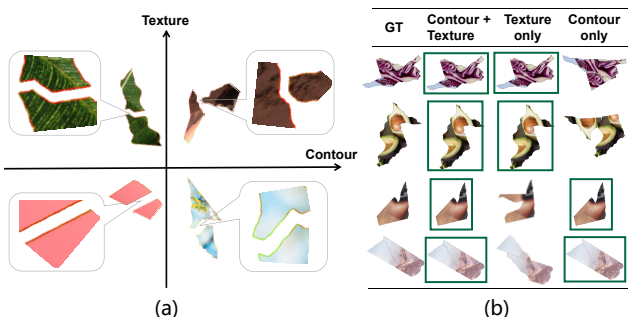


Figure 9. Visual analysis of Texture/Contour. (a) We visualize the weights of texture and contour features in our network, with colors closer to red representing more use of texture features and closer to green representing more use of contour features. We can see that on edges with rich texture or close to straight lines, the weights of the extracted texture features are greater, while on edges with single texture, the weights of the contour features are greater. (b) Examples of Textur/Contour ablation study. When the local contour shapes are similar, our network has difficulty matching them correctly using only contour features, and vice versa. However, these cases can be solved when the two features are fused.

Network structures. We explore the performance of our network under different structures, as shown in Table 3.

Table 3. Results of ablation studies. Comparison of the impact of different feature fusion ways, feature modalities, and network layers employed in our proposed network on the performance of pair-searching and pair-matching tasks.

		Recall@5	Recall@10	NDCG@5	NDCG@10	RR
Fusion Way	Early fusion	0.448	0.559	0.376	0.413	0.658
	Concat	0.489	0.605	0.418	0.458	0.824
	Weighted	0.493	0.608	0.417	0.458	0.835
ResGCN	10	-	-	-	-	0.680
	14	-	-	-	-	0.835
	18	-	-	-	-	0.759
Transformer Encoder	3	0.488	0.600	0.410	0.450	-
	4	0.488	0.606	0.411	0.452	-
	5	0.493	0.608	0.417	0.458	-
Feature Modality	Contour-only	0.016	0.025	0.013	0.016	0.584
	Texture-only	0.479	0.597	0.394	0.436	0.657
	Contour + Texture	0.493	0.608	0.417	0.458	0.835

First, we test three feature fusion ways. In early fusion, instead of using two separate GCNs for feature extraction, we concatenate the two modalities and use only one GCN to learn the features. We also test using a simple concatenation to replace the self-gated fusion module. The results show that the performance of both pair-searching and -matching decreases. Additionally, we explore the impact of different numbers of layers on our network.

Texture/Contour. To study the impact of contour and texture features on the performance of our network, we conducted experiments using only one modality (either contour or texture) and compared the final results. As shown in Table 3, the comparison results indicate that both modalities perform slightly worse when used independently. When both modalities are used in conjunction, our network achieves the best performance. We also show examples of failed pair-matching when the two modalities are used individually in Figure 9 (b).

Besides, as shown in Figure 9 (a), it can be seen numerically that our network tends to assign more weight to the texture features. This is reasonable because textures usually contain richer information than the contours of image fragments, enabling the network to learn more discriminative features.

Others. We report the results of ablation studies on patch size, contour encoding, and hyperparameters in our supplementary material.

6. Conclusions and Further Work

In this paper, to tackle the image fragment pair-searching and -matching tasks, we propose a novel network, PairingNet, to deduce the adjacent segments of fragments and encode the global features of each fragment. In PairingNet, ResGCN is employed as the backbone to extract the local contour and texture features of fragments. For pair-searching, a linear transformer-based module processes these local features leveraging the contrast of paired fragments and unpaired fragments. For pair-matching, we de-

sign a weighted fusion module to dynamically fuse the extracted local contour and texture features. Furthermore, to provide a foundation for learning-based methods, we design a cutting algorithm to generate a dataset by simulating real image fragments. Comprehensive experiments are conducted on our generated dataset, the results of which demonstrate the effectiveness of our PairingNet in comparison to existing methods. In further work, we will continue to explore the application of our PairingNet in real scenarios, such as archaeological fragments.

A. Generated Dataset Examples

The cutting algorithm we designed is implemented in Python and takes an average of 11 seconds to tear a complete image into the required fragments. We show more cutting results generated in our dataset, as shown in Figure 10. The fragments we generate are rich in shapes and patterns and have a similar effect to shredding by hand.

B. Contour Encoding Details

We design three contour encodings as shown in Figure 11: (1) Edge-only; (2) Inside-Outside; (3) Edge + Inside-Outside. Encoding (1) describes where the contour is located. Encoding (2) describes which positions are fragmented parts and which are not. Encoding (3) combines the above two encodings. We also test the impact of different patch sizes on performance in the ablation studies.

C. Ablation Study

We provide detailed ablation study results as shown in Table 4.

C.1. Network Details

Contour Encoding Methods. We tested the impact of three contour encodings on the pair-matching task. Experimental results show that Encoding (1) Edge-only achieves the best matching performance.

Patch Size. We use a patch size of 7×7 to encode contours in our proposed network. We also tested the impact of patch sizes 3×3 and 11×11 on the pair-matching task; however, they did not achieve better performance.

ResGCN Layer. The ResGCN encoder in both branches of our network contains 14 GCN layers, with each node connecting 8 nodes on both sides of its vicinity. The length of the contour points is unified to the maximum length 2900, and zero-padding is used. We tested the impact of the 10 and 18 layers on the pair-matching task. When using more or fewer GCN layers, the pair-matching performance of our model decreases. This shows that simply increasing the capacity of the encoder does not always lead to better performance.

Transformer Encoder Layer. The linear transformer encoder in our network contains 5 layers, and the input length is truncated to 1408. We tested the impact of 3 and 4 layers on pair-searching performance. When using more layers of Transformer Encoder, the network has better searching performance. Due to computational resource constraints, we did not further test higher capacities.

Fusion way. In addition to the shortened table, we also provide all results of the three feature fusion methods to show the impact on our proposed network.

Feature Fusion in Pair-searching Module. Due to better performance, we replaced the element-wise addition operation of the feature fusion in the pair-searching module with channel-wise concatenation.

Parameters in Loss Functions. For the two-step training strategy, we first train the feature extraction network and the pair-matching module by our pair-matching loss. Freeze them and then train the pair-searching module by our pair-searching loss. In the Focal loss, the balancing weights β_1 was set to 0.55 and the decay factor γ was set to 8. We also tested two other sets of parameter combinations, $\beta_1 = 0.25$, $\gamma = 4$ and $\beta_1 = 0.4$, $\gamma = 6$, respectively. In the InfoNCE loss, we set the temperature to 0.12. We also tested the impact of setting the temperature to 0.07 and 0.2. We chose the parameters that achieved optimal performance.

C.2. Reduce Texture Information

In the ablation study of feature modality, we can see that texture features contribute more performance compared to contour features. To further verify the necessity of extracting contour features, we processed the original RGB fragments into grayscale and binarized them using the Canny edge detector (Figure 12) to reduce the texture information and show the impact on our tasks.

The evaluation results got worse, since the texture information is lost in grayscale fragments and binarized ones have almost no texture features. Then, when we input binarized fragments, the contour-only modality achieved the best performance, showing the effectiveness of contour features.

C.3. Others

Backbone. We tested another commonly used graph-based network, Graph U-Nets [17], as our backbone; however, the performance decreased.

Train Pair-searching module using Pair-matching Features. We also tested using the features fused by the pair-matching module to train the pair-searching module; however, the performance declined. This shows that the features required for pair-searching and -matching tasks are not exactly the same.

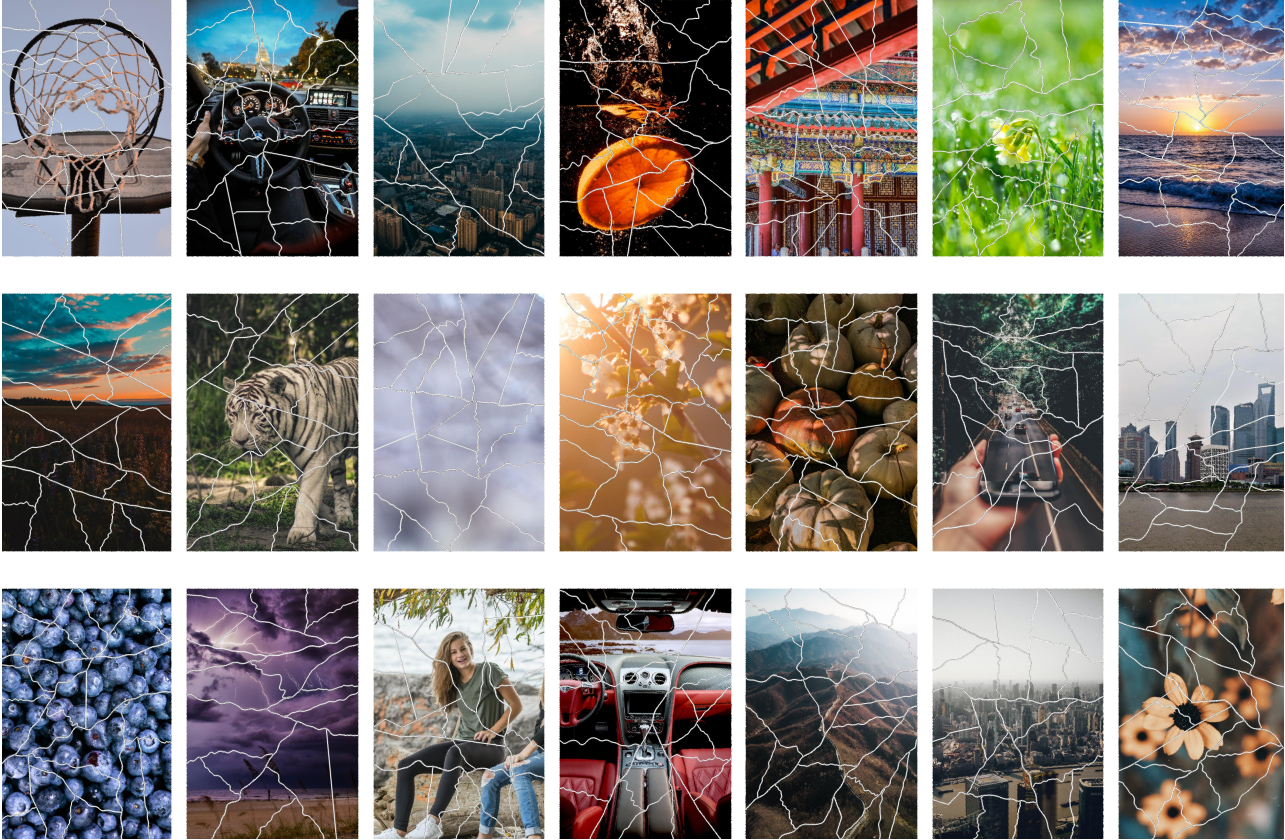


Figure 10. Cutting examples in our generated dataset, which are rich in shapes and patterns.

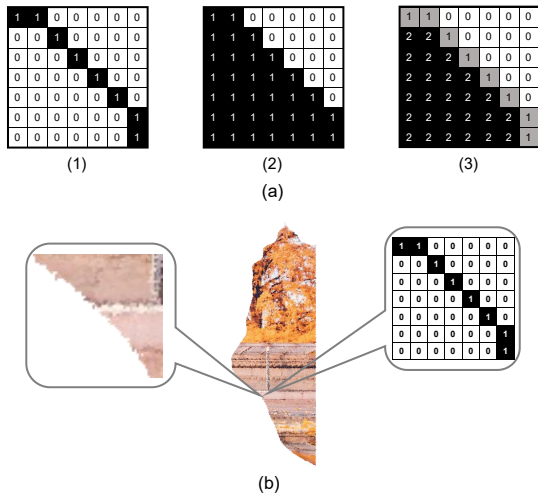


Figure 11. Coutour encodings. (a) Three contour encodings: (1) Edge-only, (2) Inside-Outside, (3) Edge + Inside-Outside. (b) Example of Edge-only encoding we used.

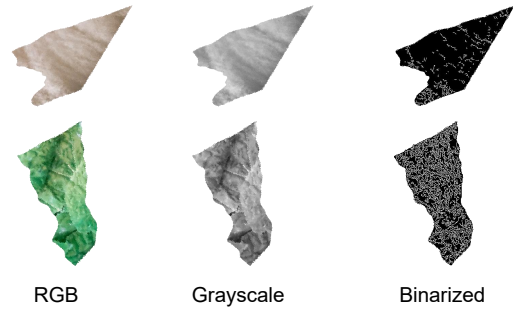


Figure 12. Examples of the RGB, grayscale, and binarized fragments.

C.4. Visualization

We visualize pair-matching correspondences between the fragments predicted by our network, as shown in Figure 13. The correct matching points are connected by green lines, while incorrectly predicted matching points are connected by red lines. For any two fragments, in addition to the optimal matching points, there are also suboptimal matching points that may interfere with the network performance. For example, the locations connected by the red

Table 4. Detailed results of ablation studies.

		Recall@5	Recall@10	Recall@20	NDCG@5	NDCG@10	NDCG@20	RR \uparrow	HD \downarrow	RE \downarrow	NTE \downarrow	
Contour Encoding	(1)	-	-	-	-	-	-	0.835	43.180	0.352	7.735×10^{-4}	
	(2)	-	-	-	-	-	-	0.695	75.423	0.576	13.716×10^{-4}	
	(3)	-	-	-	-	-	-	0.671	84.982	0.641	15.078×10^{-4}	
Patch Size	3 \times 3	-	-	-	-	-	-	0.714	72.477	0.566	13.291×10^{-4}	
	7 \times 7	-	-	-	-	-	-	0.835	43.180	0.352	7.735×10^{-4}	
	11 \times 11	-	-	-	-	-	-	0.663	84.751	0.649	15.306×10^{-4}	
ResGCN Layer	10	-	-	-	-	-	-	0.68	81.163	0.610	14.847×10^{-4}	
	14	-	-	-	-	-	-	0.835	43.180	0.352	7.735×10^{-4}	
	18	-	-	-	-	-	-	0.759	62.51	0.484	11.165×10^{-4}	
Transformer Encoder Layer	3	0.488	0.600	0.697	0.410	0.450	0.476	-	-	-	-	
	4	0.488	0.606	0.711	0.411	0.452	0.481	-	-	-	-	
	5	0.493	0.608	0.714	0.417	0.458	0.487	-	-	-	-	
Fusion Way	Early fusion	0.448	0.559	0.672	0.376	0.413	0.446	0.658	85.558	0.636	15.547×10^{-4}	
	Concat	0.489	0.605	0.706	0.418	0.458	0.486	0.824	45.521	0.359	8.269×10^{-4}	
	Weighted	0.493	0.608	0.714	0.417	0.458	0.487	0.835	43.180	0.352	7.735×10^{-4}	
Feature Fusion in Pair-searching Module	Element-wise Addition	0.489	0.605	0.706	0.418	0.459	0.486	-	-	-	-	
	Channel-wise Concatenation	0.493	0.608	0.714	0.417	0.458	0.487	-	-	-	-	
Focal Loss Paramaters	$\beta_1=0.25, \gamma=4$	-	-	-	-	-	-	0.514	124.88	0.886	21.972×10^{-4}	
	$\beta_1=0.4, \gamma=6$	-	-	-	-	-	-	0.752	65.181	0.505	11.631×10^{-4}	
	$\beta_1=0.55, \gamma=8$	-	-	-	-	-	-	0.835	43.180	0.352	7.735×10^{-4}	
InfoNCE Temperature	0.07	0.485	0.593	0.692	0.413	0.451	0.478	-	-	-	-	
	0.12	0.493	0.608	0.714	0.417	0.458	0.487	-	-	-	-	
	0.2	0.474	0.579	0.679	0.394	0.430	0.457	-	-	-	-	
Feature Modality	RGB	Contour-only	0.016	0.025	0.049	0.013	0.016	0.023	0.584	122.953	0.846	19.806×10^{-4}
		Texture-only	0.479	0.597	0.705	0.394	0.436	0.466	0.657	85.438	0.684	15.872×10^{-4}
		Contour+Texture	0.493	0.608	0.714	0.417	0.458	0.487	0.835	43.180	0.352	7.735×10^{-4}
	Grayscale	Contour-only	0.018	0.032	0.053	0.013	0.019	0.025	0.535	138.238	0.942	22.314×10^{-4}
		Texture-only	0.258	0.355	0.470	0.205	0.24	0.271	0.633	94.706	0.700	17.147×10^{-4}
		Contour+Texture	0.281	0.379	0.487	0.226	0.261	0.291	0.833	44.917	0.365	7.738×10^{-4}
	Binarized	Contour-only	0.086	0.124	0.184	0.069	0.083	0.100	0.562	126.609	0.857	20.459×10^{-4}
		Texture-only	0.027	0.048	0.082	0.019	0.027	0.037	0.000	232.263	1.562	42.034×10^{-4}
		Contour+Texture	0.036	0.051	0.083	0.029	0.034	0.043	0.553	127.997	0.888	21.072×10^{-4}
Use Graph U-Nets as Backbone		-	-	-	-	-	-	0.629	97.111	0.744	17.001×10^{-4}	
Train Pair-searching module using Pair-matching Features		0.434	0.535	0.632	0.358	0.392	0.419	-	-	-	-	

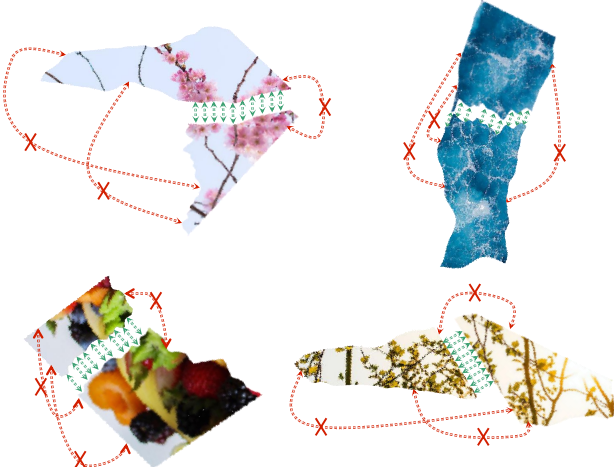


Figure 13. Pair-matching correspondences. Lines show the correspondences predicted by our network between fragment pairs. Green is used to indicate correctly paired points, while red is used to indicate incorrectly paired points.

lines in Figure 13 also exhibit matchable local contours or textures. Only a sufficiently high-performance network can predict as many correct matching points as possible and minimize the interference of sub-optimal matching points on the results.

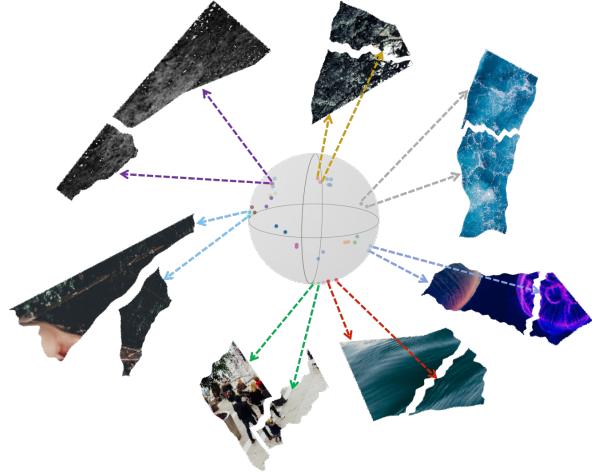


Figure 14. Visualization of the features extracted by our pair-searching module. The paired fragments are represented by the same color.

We perform dimensionality reduction visualization on the features extracted by our network to show the effectiveness of contrastive loss in the pair-searching task. Compared with Principal Component Analysis (PCA), which prefers to maintain the global structure of feature space, and

t-SNE, which focuses on maintaining the local structure, we select PaCMAP [42], a dimensionality reduction technique that preserves both global and local structures of the feature space, to reduce the features extracted by the pair-searching module to three dimensions. Subsequently, we normalize the features of each fragment and map them onto the surface of the unit sphere. We show examples in Figure 14. We can see that the features of fragment pairs represented by the same color points are close to each other, while the features of different pairs are pushed further apart.

C.5. More Comparison Results

We present more results of our network and comparison methods on pair-searching and -matching tasks, as shown in Figures 15 and 16. It can be intuitively seen that in the pair-matching task, the results obtained by our method are closer to GT, while the comparison method produces many inaccurate results. In the pair-searching task, whether it is one-to-one matching or one-to-many matching, our method can find the target fragments in the Top 5 search results. The comparison method can only find a part of the matching target fragments, and sometimes it cannot even find correct target fragments in the Top 5 search results. In the pair-searching task, our network finds the paired fragments in the Top 5 search results, whether it is one-to-one matching or one-to-many matching. However, the comparison methods can only find a part of the matching target fragments, and even cannot find correct target fragments in the Top 5. In the pair-matching task, the results obtained by our network are closer to GT, while the comparison methods produce inaccurate results.

References

- [1] Roy Abitbol, Ilan Shimshoni, and Jonathan Ben-Dov. Machine learning based assembly of fragments of ancient papyrus. *Journal on Computing and Cultural Heritage (JOCCH)*, 14(3):1–21, 2021. 1, 2
- [2] Dov Bridger, Dov Danon, and Ayellet Tal. Solving jigsaw puzzles with eroded boundaries. In *Proceedings of the IEEE/CVF Conference on Computer Vision and Pattern Recognition*, pages 3526–3535, 2020. 1, 2
- [3] Lisa Gottesfeld Brown. A survey of image registration techniques. *ACM computing surveys (CSUR)*, 24(4):325–376, 1992. 1
- [4] Ingo Joseph Bruno Joseph and Daniel Frese. Pexels. <https://www.pexels.com/>, 2023. 5
- [5] Róbert Busa-Fekete, György Szarvas, Tamás Elteto, and Balázs Kégl. An apple-to-apple comparison of learning-to-rank algorithms in terms of normalized discounted cumulative gain. In *ECAI 2012-20th European Conference on Artificial Intelligence: Preference Learning: Problems and Applications in AI Workshop*, volume 242. Ios Press, 2012. 6
- [6] J. Chen, M. Tian, X. Qi, W. Wang, and Y. Liu. A solution to reconstruct cross-cut shredded text documents based on constrained seed k-means algorithm and ant colony algorithm. *Expert Systems with Applications*, 127(AUG.):35–46, 2019. 2
- [7] Ting Chen, Simon Kornblith, Mohammad Norouzi, and Geoffrey Hinton. Simclr: A simple framework for contrastive learning of visual representations. In *International Conference on Learning Representations*, volume 2, 2020. 4
- [8] Yun-Chun Chen, Haoda Li, Dylan Turpin, Alec Jacobson, and Animesh Garg. Neural shape mating: Self-supervised object assembly with adversarial shape priors. In *Proceedings of the IEEE/CVF Conference on Computer Vision and Pattern Recognition*, pages 12724–12733, 2022. 2
- [9] Xing Cheng, Hezheng Lin, Xiangyu Wu, Fan Yang, and Dong Shen. Improving video-text retrieval by multi-stream corpus alignment and dual softmax loss. *arXiv preprint arXiv:2109.04290*, 2021. 4
- [10] Taeg Sang Cho, Shai Avidan, and William T Freeman. A probabilistic image jigsaw puzzle solver. In *2010 IEEE Computer society conference on computer vision and pattern recognition*, pages 183–190. IEEE, 2010. 2
- [11] Helena Cristina da Gama Leitao and Jorge Stolfi. A multiscale method for the reassembly of two-dimensional fragmented objects. *IEEE Transactions on Pattern Analysis and Machine Intelligence*, 24(9):1239–1251, 2002. 1, 2
- [12] Niv Derech, Ayellet Tal, and Ilan Shimshoni. Solving archaeological puzzles. *Pattern Recognition*, 119:108065, 2021. 2
- [13] Martin A Fischler and Robert C Bolles. Random sample consensus: a paradigm for model fitting with applications to image analysis and automated cartography. *Communications of the ACM*, 24(6):381–395, 1981. 5
- [14] Herbert Freeman and L Garder. Apictorial jigsaw puzzles: The computer solution of a problem in pattern recognition. *IEEE Transactions on Electronic Computers*, (2):118–127, 1964. 1, 2
- [15] Thomas Funkhouser, Hijung Shin, Corey Toler-Franklin, Antonio García Castañeda, Benedict Brown, David Dobkin, Szymon Rusinkiewicz, and Tim Weyrich. Learning how to match fresco fragments. *Journal on Computing and Cultural Heritage (JOCCH)*, 4(2):1–13, 2011. 1, 2
- [16] Andrew C Gallagher. Jigsaw puzzles with pieces of unknown orientation. In *2012 IEEE Conference on computer vision and pattern recognition*, pages 382–389. IEEE, 2012. 2
- [17] Hongyang Gao and Shuiwang Ji. Graph u-nets. In *international conference on machine learning*, pages 2083–2092. PMLR, 2019. 9
- [18] Yulan Guo, Mohammed Bennamoun, Ferdous Sohel, Min Lu, Jianwei Wan, and Ngai Ming Kwok. A comprehensive performance evaluation of 3d local feature descriptors. *International Journal of Computer Vision*, 116:66–89, 2016. 1
- [19] Shir Gur and Ohad Ben-Shahar. From square pieces to brick walls: The next challenge in solving jigsaw puzzles. In *Proceedings of the IEEE International Conference on Computer Vision*, pages 4029–4037, 2017. 2
- [20] Je Hyeong Hong, Seong Jong Yoo, Muhammad Arshad Zee-shan, Young Min Kim, and Jinwook Kim. Structure-from-sherds: Incremental 3d reassembly of axially symmetric pots

- from unordered and mixed fragment collections. In *Proceedings of the IEEE/CVF International Conference on Computer Vision*, pages 5443–5451, 2021. 2
- [21] Hui Huang, Kangxue Yin, Minglun Gong, Dani Lischinski, Daniel Cohen-Or, Uri M Ascher, and Baoquan Chen. ”mind the gap”: tele-registration for structure-driven image completion. *ACM Trans. Graph.*, 32(6):174–1, 2013. 2
- [22] Qi-Xing Huang, Simon Flöry, Natasha Gelfand, Michael Hofer, and Helmut Pottmann. Reassembling fractured objects by geometric matching. In *ACM SIGGRAPH 2006 Papers*, pages 569–578. 2006. 1, 2
- [23] Benjamin Jones, Dalton Hildreth, Duowen Chen, Ilya Baran, Vladimir G Kim, and Adriana Schulz. Automate: A dataset and learning approach for automatic mating of cad assemblies. *ACM Transactions on Graphics (TOG)*, 40(6):1–18, 2021. 2
- [24] Weixin Kong and Benjamin B Kimia. On solving 2d and 3d puzzles using curve matching. In *Proceedings of the 2001 IEEE Computer Society Conference on Computer Vision and Pattern Recognition. CVPR 2001*, volume 2, pages II–II. IEEE, 2001. 2
- [25] Nikolas Lamb, Cameron Palmer, Benjamin Molloy, Sean Banerjee, and Natasha Kholgade Banerjee. Fantastic breaks: A dataset of paired 3d scans of real-world broken objects and their complete counterparts. In *Proceedings of the IEEE/CVF Conference on Computer Vision and Pattern Recognition*, pages 4681–4691, 2023. 2
- [26] Canyu Le and Xin Li. Jigsawnet: Shredded image reassembly using convolutional neural network and loop-based composition. *IEEE Transactions on Image Processing*, 28(8):4000–4015, 2019. 2, 6
- [27] Guohao Li, Matthias Muller, Ali Thabet, and Bernard Ghanem. Deepgcns: Can gcns go as deep as cnns? In *Proceedings of the IEEE/CVF international conference on computer vision*, pages 9267–9276, 2019. 3
- [28] Yang Li and Tatsuya Harada. Leopard: Learning partial point cloud matching in rigid and deformable scenes. In *Proceedings of the IEEE/CVF Conference on Computer Vision and Pattern Recognition*, pages 5554–5564, 2022. 4
- [29] Hairong Liu, Shengjiao Cao, and Shuicheng Yan. Automated assembly of shredded pieces from multiple photos. *IEEE transactions on multimedia*, 13(5):1154–1162, 2011. 2
- [30] Krystian Mikolajczyk and Cordelia Schmid. A performance evaluation of local descriptors. *IEEE transactions on pattern analysis and machine intelligence*, 27(10):1615–1630, 2005. 1
- [31] Aaron van den Oord, Yazhe Li, and Oriol Vinyals. Representation learning with contrastive predictive coding. *arXiv preprint arXiv:1807.03748*, 2018. 4
- [32] Thiago M. Paixao, Mcs Boeres, Coa Freitas, and T. Oliveira-Santos. Exploring character shapes for unsupervised reconstruction of strip-shredded text documents. *IEEE Transactions on Information Forensics and Security*, pages 1–1, 2018. 2
- [33] Marie-Morgane Paumard, David Picard, and Hedi Tabia. Image reassembly combining deep learning and shortest path problem. In *Proceedings of the European conference on computer vision (ECCV)*, pages 153–167, 2018. 1, 2
- [34] Dolev Pomeranz, Michal Shemesh, and Ohad Ben-Shahar. A fully automated greedy square jigsaw puzzle solver. In *CVPR 2011*, pages 9–16. IEEE, 2011. 1, 2
- [35] F Richter, C. X Ries, N Cebren, and R Lienhart. Learning to reassemble shredded documents. *IEEE Transactions on Multimedia*, 15(3):582–593, 2013. 2
- [36] Ignacio Rocco, Mircea Cimpoi, Relja Arandjelović, Akihiko Torii, Tomas Pajdla, and Josef Sivic. Neighbourhood consensus networks. *Advances in neural information processing systems*, 31, 2018. 4
- [37] Silvia Sellán, Yun-Chun Chen, Ziyi Wu, Animesh Garg, and Alec Jacobson. Breaking bad: A dataset for geometric fracture and reassembly. *Advances in Neural Information Processing Systems*, 35:38885–38898, 2022. 2
- [38] Kilho Son, James Hays, and David B Cooper. Solving square jigsaw puzzles with loop constraints. In *European conference on computer vision*, pages 32–46. Springer, 2014. 2
- [39] Kilho Son, James Hays, and David B Cooper. Solving square jigsaw puzzle by hierarchical loop constraints. *IEEE transactions on pattern analysis and machine intelligence*, 41(9):2222–2235, 2018. 1, 2
- [40] Efthymia Tsamoura and Ioannis Pitas. Automatic color based reassembly of fragmented images and paintings. *IEEE Transactions on Image Processing*, 19(3):680–690, 2009. 2
- [41] Sinong Wang, Belinda Z Li, Madian Khabsa, Han Fang, and Hao Ma. Linformer: Self-attention with linear complexity. *arXiv preprint arXiv:2006.04768*, 2020. 4
- [42] Yingfan Wang, Haiyang Huang, Cynthia Rudin, and Yaron Shaposhnik. Understanding how dimension reduction tools work: an empirical approach to deciphering t-sne, umap, trimap, and pacmap for data visualization. *The Journal of Machine Learning Research*, 22(1):9129–9201, 2021. 12
- [43] Ruihai Wu, Chenrui Tie, Yushi Du, Yan Zhao, and Hao Dong. Leveraging se (3) equivariance for learning 3d geometric shape assembly. In *Proceedings of the IEEE/CVF International Conference on Computer Vision*, pages 14311–14320, 2023. 2
- [44] Xi Yang, Katsutsugu Matsuyama, and Kouichi Konno. Pairwise matching of stone tools based on flake-surface contour points and normals. In *Proceedings of the Eurographics Workshop on Graphics and Cultural Heritage*, pages 125–129, 2017. 2
- [45] Shuainan Ye, Zhutian Chen, Xiangtong Chu, Kang Li, Jun-tong Luo, Yi Li, Guohua Geng, and Yingcai Wu. Puzzlefixer: A visual reassembly system for immersive fragments restoration. *IEEE transactions on visualization and computer graphics*, 29(1):429–439, 2022. 2
- [46] Guanqi Zhan, Qingnan Fan, Kaichun Mo, Lin Shao, Baoquan Chen, Leonidas J Guibas, Hao Dong, et al. Generative 3d part assembly via dynamic graph learning. *Advances in Neural Information Processing Systems*, 33:6315–6326, 2020. 2
- [47] Kang Zhang and Xin Li. A graph-based optimization algorithm for fragmented image reassembly. *Graphical Models*, 76(5):484–495, 2014. 2, 6

Fragments		Top1	Top2	Top3	Top4	Top5
Source fragment ↓ Target fragment	Ours					
	Jigsawnet					
	Rule-based					
Source fragment ↓ Target fragment	Ours					
	Jigsawnet					
	Rule-based					
Source fragment ↓ Target fragment	Ours					
	Jigsawnet					
	Rule-based					
Source fragment ↓ Target fragment	Ours					
	Jigsawnet					
	Rule-based					
Source fragment ↙ ↘ Target fragment1 Target fragment2	Ours					
	Jigsawnet					
	Rule-based					
Source fragment ↙ ↘ Target fragment1 Target fragment2	Ours					
	Jigsawnet					
	Rule-based					
Source fragment ↙ ↘ Target fragment1 Target fragment2	Ours					
	Jigsawnet					
	Rule-based					

Figure 15. Examples of pair-searching results. Our network is able to accurately identify the corresponding target fragment (high-lighted with a green box).

	Fragments	GT	Ours	Jigsawnet	Rule-based
High					
Medium					
Low					

Figure 16. Examples of pair-matching results for three difficulty levels. Our proposed network achieves satisfactory matching results.